Applied Mechanics and Materials
ISSN: 1662-7482, Vol. 915, pp 81-94
© 2023 Trans Tech Publications Ltd, Switzerland
Submitted: 2023-03-06
Revised: 2023-04-23
Accepted: 2023-05-03
Online: 2023-08-18

Thermo-Structural Response Prediction of UHTCC Control Surface for Hypersonic Cruise Vehicle

Abdullah Ghori[1,a,*], Saggam Narendar[2,b] and Yogita Dubey[2,c]

[1]Jawaharlal Nehru Technological University, Hyderabad, India
[2]Defence Research & Development Laboratory (DRDO), Hyderabad, India

[a]ammar.ghori23@outlook.com, [b]narendar@drdl.drdo.in, [c]yogita1008d@gmail.com

Keywords: Hypersonic, Aerothermodynamics, Thermal Protection System, CFD, UHTCC

Abstract. One of the most complex issues that govern the design of a hypersonic vehicle is aerodynamic heating, which is much more severe for an air-breathing vehicle as it operates within the atmosphere for longer durations. Due to the detrimental impact of aerodynamic heating on the vehicle structure, it is imperative to develop a robust thermal protection system that can protect the vehicle from high temperatures. However, the development of a sophisticated thermal protection system (TPS) for slender components is impractical and, therefore, requires a hot structure system that can operate at consequential aerothermal loads. This study aims to predict the impact of aero-heating on an ultra-high-temperature ceramic composite (UHTCC) based hot structure system of a hypersonic cruise vehicle through uncoupled thermo-structural analysis of the control surface. Validation of numerical methods implemented is done through literature comparison and grid independency tests. Furthermore, the outcomes of this study suggest that the UHTC composites are a viable choice for hot structure TPS for slender hypersonic vehicle components. In addition to this, the uncoupled approach toward multiphysics analysis of hypersonic flow was found to be computationally inexpensive and accurate enough for TPS development.

1. Introduction

The design of hypersonic vehicles is associated with a myriad of technical challenges with one of the most convoluted ones being aerodynamic heating. This phenomenon largely depends upon the geometry, orientation and flight trajectory of the vehicle. Unlike others, it poses a greater challenge to the structure of hypersonic airbreathing vehicles as they operate within the atmosphere for longer durations [1].

In 2005, Leonard et. al. performed thermal analysis for hot structure components of X-43A research vehicle for Mach 7 and 10 to predict their operability under high aerothermodynamic heating [2]. Engineering codes were used for the estimation of heating loads based on the flight trajectory which was then used for thermal and structural analysis. A similar study was presented by Wang et. al. [3] on an aerospace plane flying at Mach 4.97. Narendar et. al. performed a thermo-structural experiment to evaluate the structural integrity of the ceramic radome for a missile operating at high aerothermal loads [4]. Apart from structural efficacy, the radome was required to insulate the critical avionics from high temperatures during the flight. Manu et. al. investigated the thermo-mechanical behaviour of carbon phenolic-based TPS for the ISRO's Crew Module Atmospheric Re-entry Experiment (CARE). The thermal stresses induced in the module, due to the aerodynamic heating, were studied to predict the viability of carbon phenolic tiles as heat shields [5]. The differential expansion of components, resulting from high-temperature gradients, can seriously challenge the structure of the vehicle Figure 1 illustrates the heat transfer to the vehicle structure due to aerothermal heating). Therefore, it is imperative to develop a robust thermal protection system that can withstand high aerothermal loads developed during the hypersonic flight.

In [6], Esser et. al. provides an overview of recent developments in various thermal management concepts. The authors argue that the selection of optimal TPS depends upon the entry velocity, trajectory, shape and size of the vehicle, including the atmospheric properties. Figure 2 shows various

All rights reserved. No part of contents of this paper may be reproduced or transmitted in any form or by any means without the written permission of Trans Tech Publications Ltd, www.scientific.net. (#622236384-16/08/23,14:46:15)

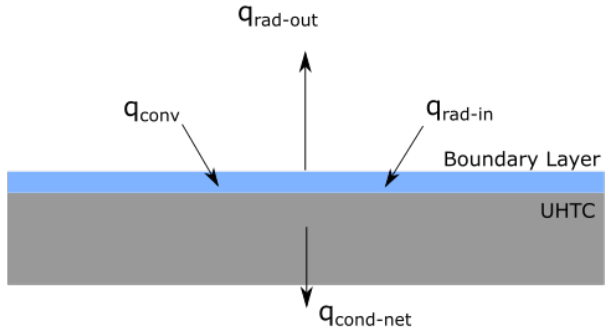


Fig. 1: Energy conservation in aerodynamic heating

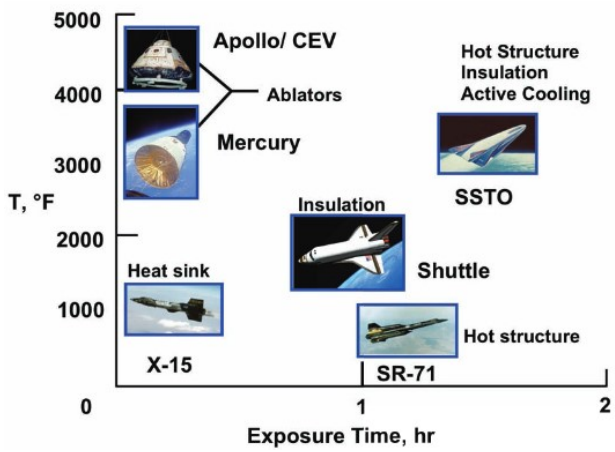


Fig. 2: Types of TPS for different hypersonic vehicles [8]

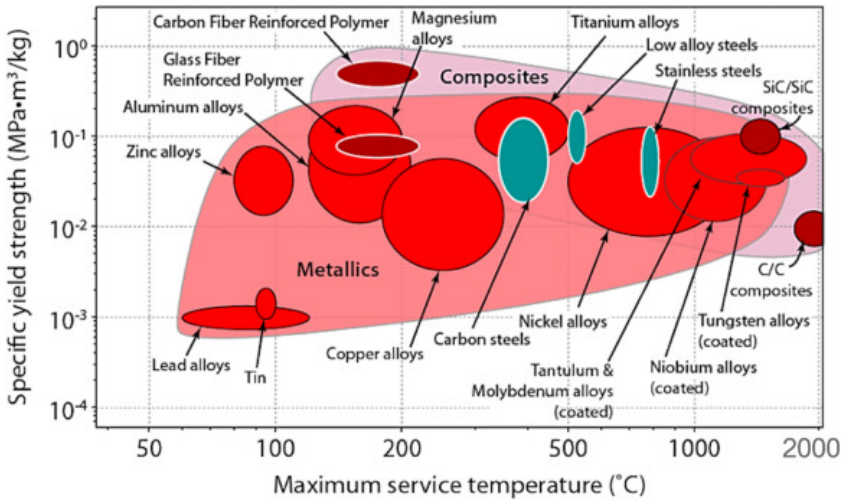


Fig. 3: Specific yield strength vs maximum service temperature for hot structure candidate materials [16]

types of TPS necessary for different flight trajectories. While the thermal insulation and ablative TPS work well for atmospheric re-entry, they are not suitable for single-stage-to-orbit (SSTO) vehicles such as the National Aerospace Plane (NASP) that are subjected to high temperatures for an extended time. Moreover, the selection of TPS is also dictated by the type of vehicle structure/component to be protected from substantial heat flux. One of the simplest, yet efficient approaches to the thermal protection system (TPS) of hypersonic cruise vehicles is the *hot structure* system. Unlike other methods, the vehicle components are designed using high-temperature materials such as super alloys, functionally graded materials (FGM), and ultra-high-temperature ceramic composites (UHTCC), to survive a high aero-heating trajectory [7]. A passive approach to thermal management is ineffective for a cruise trajectory as the primary structure would eventually overheat resulting in structural failure. On the other hand, an active cooling system is ideal for airframes and other larger vehicle structures as they require complex auxiliary equipment for their operation. A UHTCC-based hot structure system is ideal for slender components such as the nose-tip, leading edges, intake cowl and strut-based flame holders of scramjet engines that require thermal and structural stability at high temperatures [8, 9]. These composites are designed to overcome the brittleness of monolithic ceramics thus making them suitable for aerostructures [10]. As Figure 3 indicates, carbon fibre-reinforced C-SiC has been an attractive choice for hot structures, mainly due to their high rigidity, in addition to, excellent thermal and

structural stability. This composite has relatively short reinforcement fibres and inexpensive polymer precursors and is fabricated through a liquid silicon infiltration process [11, 12]. However, ceramic matrix composites (CMCs) tend to have poor thermal shock resistance (TSR) which makes it imperative to use composites having higher thermal diffusivities where temperature gradients are substantial [13]. Moreover, due to the high emissivity of these composites, the radiation-adiabatic temperature will be significantly lower than the adiabatic wall and stagnation point temperatures [14, 15].

Moreover, the hypersonic flow is associated with various complex phenomena that heavily influence the flow field around the vehicle [18, 19]. This makes the numerical study of such flows quite complicated as the classical theory of compressible flow no longer remains accurate [20]. Hence, to design a thermal protection system, it is important to accurately predict the behaviour of high-speed compressible flow and its effects on the vehicle. In [21], Sun et. al. performed a thermo-structural analysis to determine the performance of the nose cap of a hypersonic vehicle subjected to aerodynamic heating. The authors proposed a two-way multi-field coupling strategy for the exchange of simulation data between the two regions (fluid and solid) having different mesh topologies. Chen et. al. performed a similar analysis on a cylindrical leading edge by using a time-adaptive loosely coupled strategy [22]. Hence, the coupling of multi-physical simulation is a complex process wherein accurate mapping and transfer of data is the key to modelling fluid-thermal-structural interaction. However, it is a computationally expensive and time-consuming approach. Contrary to this, an uncoupled method is relatively faster and inexpensive as each analysis is carried out separately and the results of one are used as boundary conditions for the other [23]. A similar method was used by the authors for thermo-structural analysis of the nose tip and wings of X-43A RV [2]. Though this type of analysis does not predict the fluid-thermal-structural interaction, it is accurate enough for the design and analysis of thermal protection systems for hypersonic vehicles.

The primary objective of this paper is to analyse the thermo-structural behaviour of a UHTCC-based control surface for a hypersonic cruise vehicle. This study takes an uncoupled approach toward the multiphysics analysis in which the flowfield and its effects are modelled first, followed by the thermal and structural analysis. Though this method is relatively less accurate than the coupled approach, it is much faster and computationally inexpensive for the study of hot structure TPS performance. Further, a parametric analysis of hypersonic aerothermal effects on the control surface is presented to demonstrate the impact of cruise velocity on the vehicle structure.

Hypersonic aerothermal flows. Computational fluid dynamics is an indispensable tool in the design of hypersonic vehicles as there are a variety of complex numerical and physical problems associated with the hypersonic flow that must be resolved. Various sophisticated numerical methods are available to predict the aerodynamic forces and heat flux, thus expediting the design and minimizing the need for complex testing equipment [18].

Following are the Navier-Stokes equations for hypersonic viscous flows:

Continuity Equation:

$$\frac{\partial \rho}{\partial t} + \nabla.(\rho V) = 0 \tag{1}$$

Momentum Equation:

$$\rho\frac{du}{dt} = -\frac{\partial p}{\partial x} + \frac{\partial \tau_{xx}}{\partial x} + \frac{\partial \tau_{yx}}{\partial y} + \frac{\partial \tau_{zx}}{\partial z} \tag{2}$$

$$\rho\frac{dv}{dt} = -\frac{\partial p}{\partial y} + \frac{\partial \tau_{xx}}{\partial x} + \frac{\partial \tau_{xy}}{\partial yy} + \frac{\partial \tau_{zy}}{\partial z} \tag{3}$$

$$\rho\frac{dw}{dt} = -\frac{\partial p}{\partial z} + \frac{\partial \tau_{xz}}{\partial x} + \frac{\partial \tau_{yz}}{\partial y} + \frac{\partial \tau_{zz}}{\partial z} \tag{4}$$

Energy Equation:

$$\rho\frac{d}{dt}(e+\frac{V^2}{2}) = \rho q+\frac{\partial}{\partial x}\left(k\frac{\partial T}{\partial x}\right)+\frac{\partial}{\partial y}\left(k\frac{\partial T}{\partial y}\right)+\frac{\partial}{\partial z}\left(k\frac{\partial T}{\partial z}\right)+\frac{\partial}{\partial x}\left(u\tau_{xx}\right)+\frac{\partial}{\partial y}\left(u\tau_{yx}\right)+\frac{\partial}{\partial z}\left(u\tau_{zx}\right)+ \frac{\partial}{\partial x}\left(v\tau_{xx}\right)+\frac{\partial}{\partial y}\left(v\tau_{yx}\right)+\frac{\partial}{\partial z}\left(v\tau_{zx}\right)+\frac{\partial}{\partial x}\left(w\tau_{xx}\right)+\frac{\partial}{\partial y}\left(w\tau_{yx}\right)+\frac{\partial}{\partial z}\left(w\tau_{zx}\right) \quad (5)$$

These governing equations must be modified further for reacting flows to account for the energy carried by the dissociating species and ablating material.

In [24], Coakley et. al. investigated various turbulence models for their NASP program and recommended using 2-equation models – the k-ϵ model of Jones & Launder, modified by Launder & Sharma and the k-ω model proposed by Wilcox. These closure models were to be used with the mass-weighted Reynolds Averaged Compressible Navier-Stokes Equation in tensor form as mentioned above. Moreover, these formulations are not adequate and require certain corrections to predict the high-speed compressible flow accurately [25].

Aerodynamic Heating. Boundary layer heat transfer occurs on the control surface due to the deceleration of high-speed air in the viscous boundary layer leading to the conversion of kinetic energy to internal energy, contributing essentially to the convective heat transfer process. Heat then conducts into the structure from a higher temperature boundary layer resulting in a rise of control surface temperature.

The UHTC composites generally have higher emissivity. This accounts for higher rates of radiative efflux from the surface, therefore, significantly lowering the temperature of the control surface.

The energy balance for aerodynamic heat transfer is given by (Refer Figure 1);

$$\dot{q}_{cond-net} = \dot{q}_{conv} + \dot{q}_{rad-in} - \dot{q}_{rad-out} \quad (6)$$

where

$$\dot{q}_{conv} = h(T_{aw} - T_{iso}) \;\; ; \;\; \dot{q}_{rad} = \sigma\epsilon T^4 \quad (7)$$

Thermoelasticity. Due to the substantial heat flux and temperature gradients, the material undergoes differential thermal expansion causing the structure to experience high thermal stresses and deflections [8]. The governing equations used for the thermo-structural analysis explain the law obeyed by the internal temperature distribution and the stresses due to aerothermal loads.

$$\rho_s c_p\frac{\partial T}{\partial t} - \frac{\partial}{\partial x_i}\left(k_i\frac{\partial T}{\partial x_i}\right) - \sigma_{ij}\frac{\partial \varepsilon_{ij}}{\partial t} = q \quad (8)$$

where σ_{ij} is the thermal stress tensor and ε_{ij} thermal strain. ρ_s is the material density. One of the prime objectives of the hot structure design is to prevent the formation of excessive stresses and minimize plastic deformation [21].

2. Methodology

Reference geometry. The hypersonic vehicle geometry referenced for the control surface design is shown in Figure 4. This geometry was considered by Dharavath et. al. [17]. The plan and side view show the sweep-back angle and thickness of the vehicle, respectively. The geometry was designed using Autodesk Inventor and pre-processed in SpaceClaim.

A multi-material UHTCC-based control surface was designed with a span of 0.75W and an overall chord length of 2.45W as shown in Figure 5. Additionally, the maximum thickness of the control surface was considered to be 0.095W. The sweep-back angle of $\Lambda \sim 64°$ was taken as it results in reduced drag and heat flux on the leading edge. Since the leading edge experienced profound shock-induced heat flux, a ZrB_2-based SiC composite was used to reduce thermal shock due to high-temperature gradients. This type of CMC has excellent thermal diffusivity which can prevent the localization of

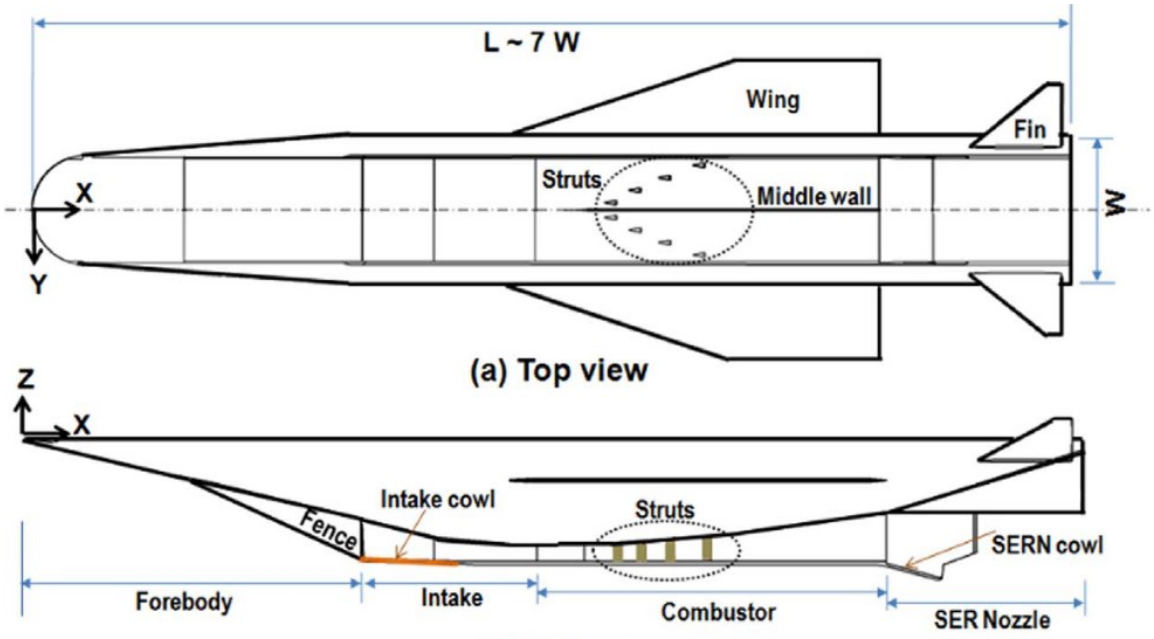


Fig. 4: Schematic of a typical hypersonic cruise vehicle [17]

thermal loads on the leading edge tip. A carbon fibre-reinforced C-SiC (C/C-SiC) composite was used for the body of the control surface as it possesses excellent thermophysical properties and low density. Additionally, it also has a lower coefficient of thermal expansion which allows it to operate at high temperatures for long durations without substantial deformation (Table 1). A paraboloid-shaped computational domain was prepared for CFD analysis comprising two local refinement regions as shown in Figure 6. High-resolution computational grids were used in these regions for higher accuracy with low computational costs.

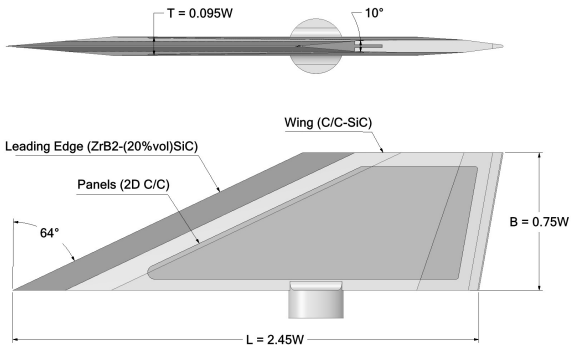


Fig. 5: Schematic of control surface for typical hypersonic cruise vehicle

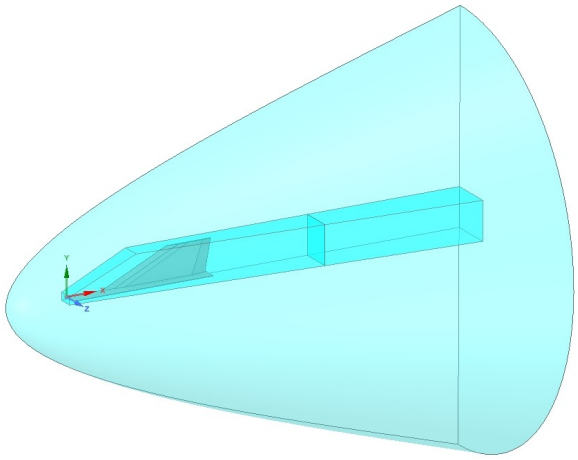


Fig. 6: Flow domain for CFD analysis

Computational grid and numerical study. The computational grid prepared for CFD analysis comprised about 1.13 million structured (poly-hexcore) elements with the size of $2.5\text{x}10^{-3}$ m in the refinement region and $40\text{x}10^{-3}$ m in the far-field as shown in Figure 7. The mesh size around the control surface was refined to accurately model near-wall effects and capture the shock waves. Further, a mesh for finite element analysis was generated having approximately 248,000 elements as shown in Figure 8. The hypersonic flow around the wing was simulated using ANSYS Fluent. The CFD analysis was performed for a hypersonic cruise trajectory with a flight velocity of Mach 8 over an altitude of 30 km (Table 2). The k-ω SST model, with compressibility and corner flow corrections, was used for

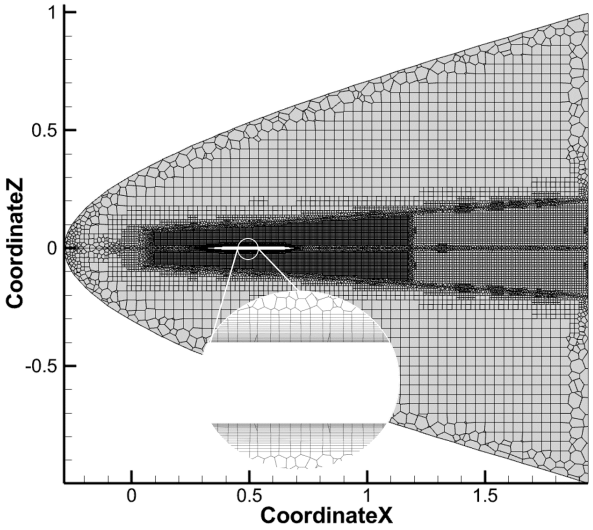


Fig. 7: Computational grid for CFD with an enhanced view of boundary layer

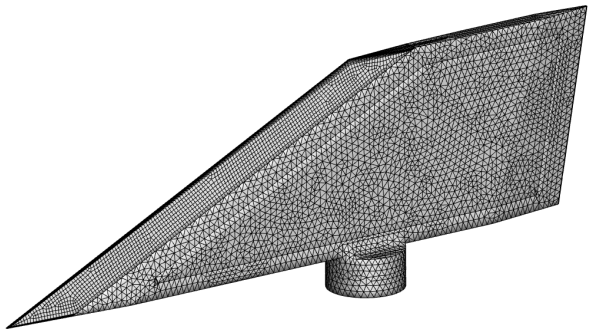


Fig. 8: Computational grid for thermo-structural analysis

Table 1: Material Properties for Control Surface Hot Structure

Property	$ZrB_2 - (20\%vol)SiC$ [26, 27]	C/C-SiC [28]	2D C/C [29, 30]
Density (kg/m^3)	5570	1870	1690
Thermal Conductivity (W/mK) RT	99	13	20-50
Heat Capacity (J/kgK) RT	460	1150	0.85
Emissivity	0.75	0.80	0.86
Young's Modulus (GPa)	518	110	90
Poisson's Ratio	0.13	0.3	0.026
Tensile Strength (MPa)	340	180	180
Thermal Expansion Coefficient (K) RT	$4.0x10^{-6}$	$2.25x10^{-6}$	$1.9x10^{-6}$

Table 2: Flight Conditions

Altitude (km)	Mach number	Temperature (K)	Pressure (Pa)
30	8.0	231.35	1189.2

turbulence closure to predict viscous effects. A least square cell-based spatial discretization scheme was used along with second-order upwind gradients for momentum and energy transfer. An implicit formulation with Roe-FDS flux was found to yield optimal results for high-speed compressible flow around the control surface. The grid size near the wall was resolved for y+ values close to one by varying initial cell layer thicknesses for different sections of the control surface. The results of steady-state CFD analysis were then mapped for a coupled thermo-structural simulation to study the structural response of the wing to aerothermal loads. The simulation was performed for a duration of 120 s using ANSYS Mechanical.

Grid convergence study. The grid convergence study was performed for adiabatic wall analysis. The optimal computational grid required for the aerothermal study was developed iteratively through varying grid sizes and element counts. The variation in leading-edge wall temperature was used as a criterion for evaluating the grid convergence. The aberrations in leading-edge temperature due to mesh refinement in the flow domain and inflation layer were found minimal and well within the tolerance limit of 2%. This indicated that the mesh used for aerothermal analysis was converged. Figure 9 shows a variation of leading edge wall temperature across dimensionless distance $\bar{X} = x/L$ for different

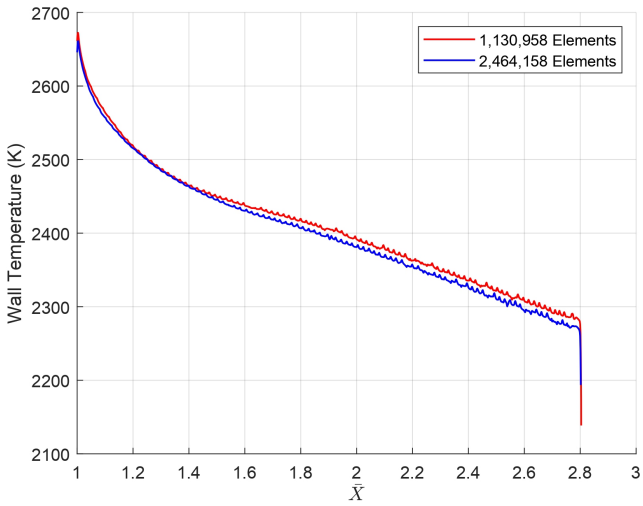


Fig. 9: Comparison of leading edge wall temperature for different computational grid size

computational grids. The initial mesh comprised about 1.13 million elements with 20 inflation layers having an average y+ of 0.74. This mesh was further refined to 2.46 million elements with 30-35 inflation layers having similar y+ values.

3. Results and Discussion

The results of CFD analysis showed the formation of a strong oblique shock at the leading edge having a shock angle (β) of 15^o (Figure 10 and 11). The peak values of temperature and heat flux were found at the stagnation region on the leading edge tip. The adiabatic wall temperature in this region was observed to be 2670 K which declined to roughly 2280 K downstream (Figure 12). In addition to this, the wing-body junction also experienced corner flow heating due to the formation of horseshoe vortices.

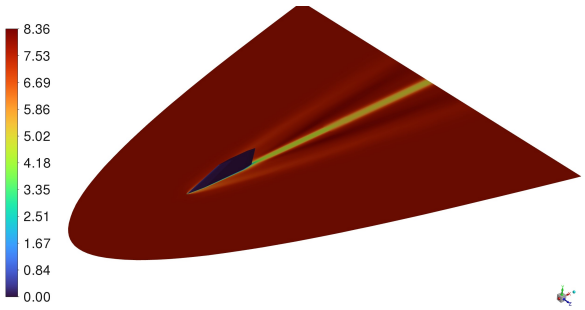


Fig. 10: Contours of Mach number

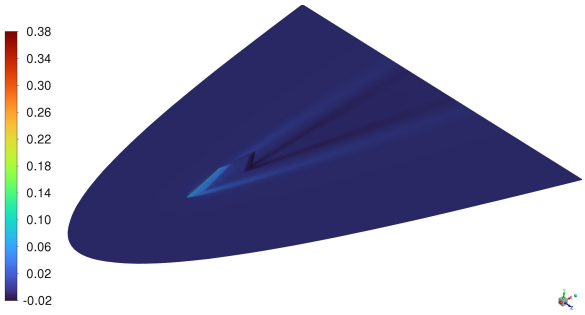


Fig. 11: Contours of pressure coefficient

Further, the Mach number plummeted to 6.18 across the shockwave, gradually increasing to 7.07 after passing through the first expansion wave and finally reaching 8.0 as the flow passed through the second expansion wave. Conversely, other flow parameters such as the pressure, density, and temperature increased substantially across the shockwave. Variation of different transport properties was observed as the temperature of flow in the boundary layer and across the shockwave exceeded 800 K. The control surface was subjected to a maximum shear stress of 2.38 kPa at the leading edge that tailed off to an average of 483.68 Pa. In addition to this, a maximum skin friction coefficient of $C_f = 0.013$ was estimated at the control surface.

The results of CFD simulation were used in transient thermal analysis where the temperature distribution and total heat flux in the structure were analysed. A parabolic increase in wall temperature

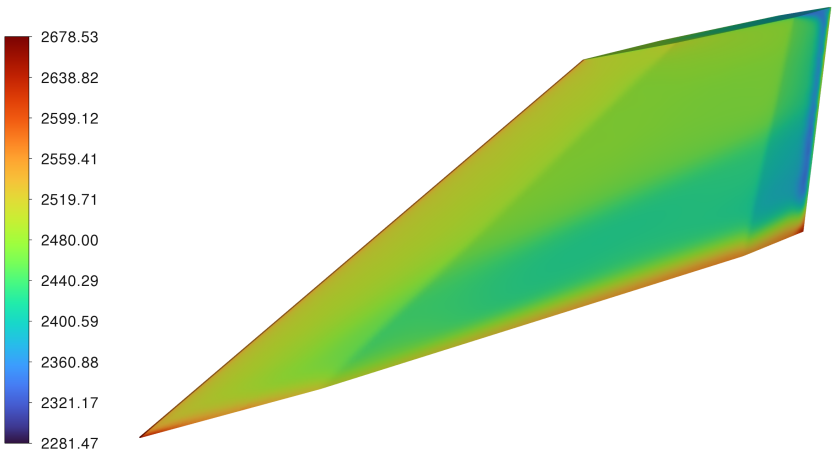
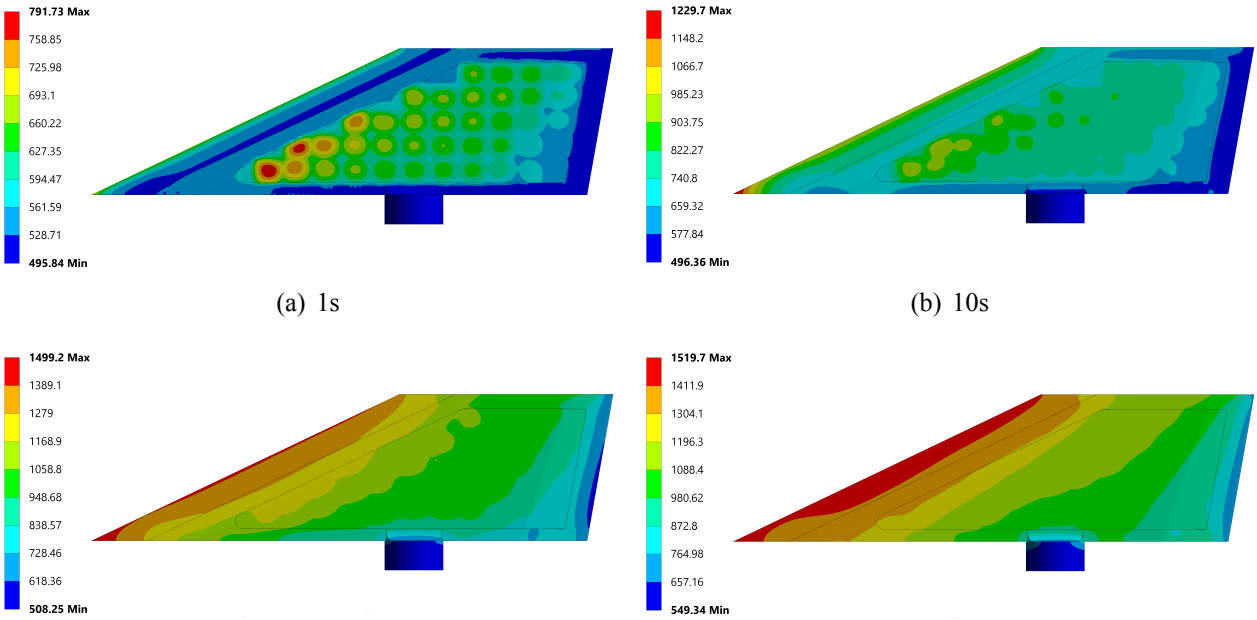


Fig. 12: Contours of adiabatic wall temperature



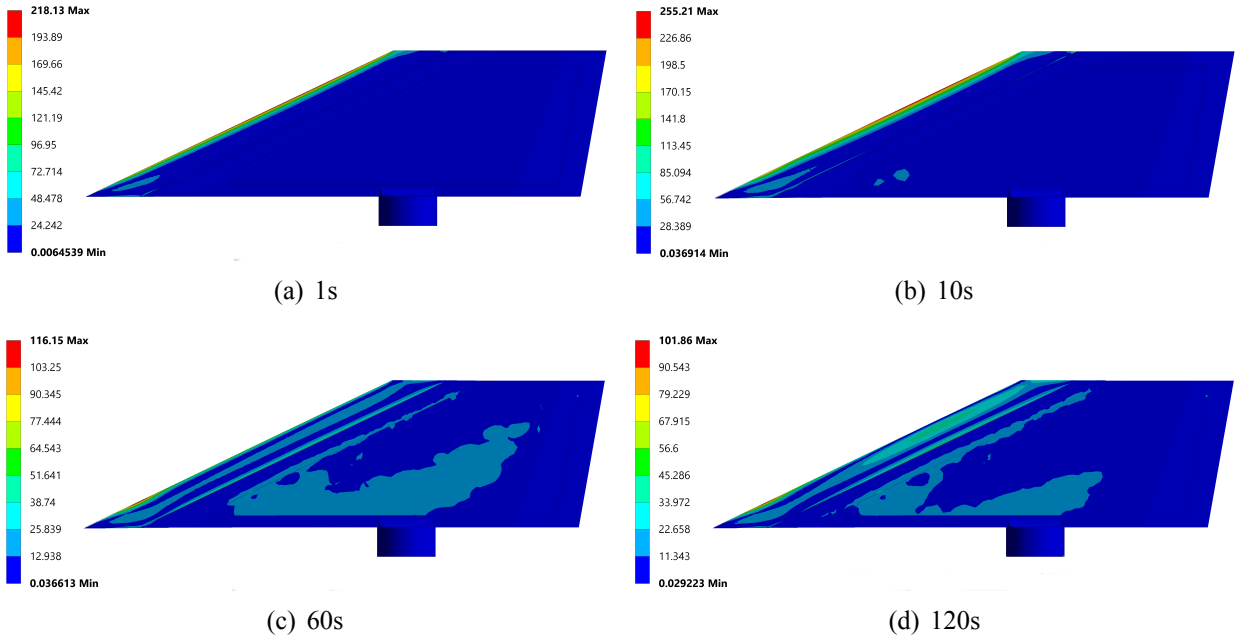
(a) 1s (b) 10s

(c) 60s (d) 120s

Fig. 13: Temperature distribution in control surface (K)

was seen which plateaued to 1500 K at around 100s as indicated in Figure 15. The temperature contours in Figure 13 show the rise and distribution of control surface temperature over time. As evident from these contours, the leading edge experiences a peak temperature of 1500 K that decreases gradually downstream. Initially, the skin panel of the control surface experienced localized heating due to the presence of cavities. This high temperature, then diffused throughout the structure over time. The heat flux to the control surface was 287 W/cm^2. The leading edge rapidly attained temperature equilibrium relative to the other components of the wing due to the higher thermal diffusivity of the $ZrB_2-(20\%vol)SiC$ composite.

The control surface undergoes thermal expansion due to severe aerodynamic heating, as a result of which the structure operates constantly at high stresses during the flight. Since the control surface was initially exposed to high-temperature gradients, it experienced high tensile stresses at the tip of the leading edge. As evident from the equivalent stress contours in Figures 14 and 16, the peak stress at the tip was 255 MPa and, with time, this value plummeted to 14 MPa. The skin panels did not experience significant stresses as the CTE of C/C-SiC and 2D C/C is nearly the same. The stress in the body of the wing continued to rise steadily while it plateaued in the case of skin panels. Moreover,



(a) 1s (b) 10s

(c) 60s (d) 120s

Fig. 14: Contours of equivalent stress (MPa)

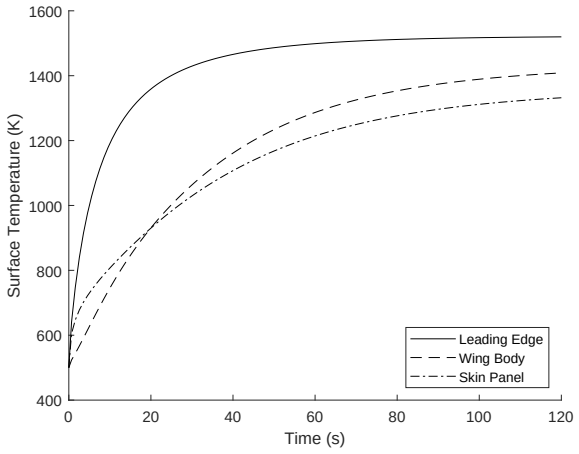


Fig. 15: Evolution of surface temperature with time

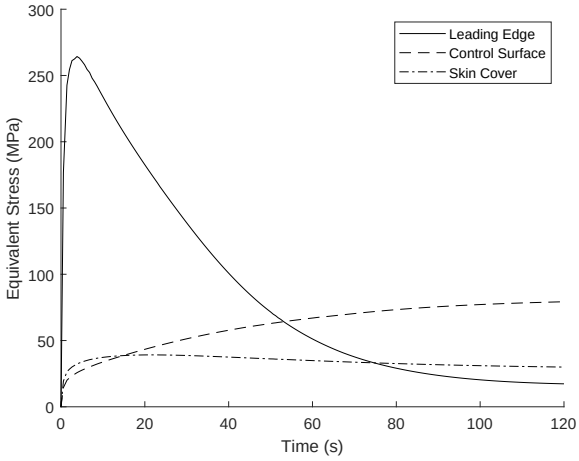


Fig. 16: Evolution of equivalent stress with time

the highest value of strain at the leading edge was around $7.48\text{x}10^{-4}$ m/m. Additionally, the stresses induced by aerothermal effects resulted in a maximum displacement of 1.7 mm as shown in Figure 17.

Performing a transient thermal simulation for a cruise trajectory of Mach 8, gave an insight into heat flux and temperature variation in the structure. Surface radiative cooling played a key role in preventing structure overheating. The temperature attained by the surface was lower than the adiabatic wall temperature as a considerable portion of heat flux was lost by radiation. This effect will be more substantial at higher wall temperatures as it depends on the fourth power of absolute wall temperature. The structural analysis indicated that the stresses induced due to thermal expansion were well within the strength limits of composites. The overall deformation observed in the control surface was also found to be minimal. The performance of the wing structure was further studied for different flight velocities over the same altitude. Figures 18 and 19 indicate the variation of surface temperature and heat flux with flight Mach number respectively. The equivalent stress and maximum displacement were also observed to increase with flight velocity (Figure 20 and 21). It was found that the aerothermal

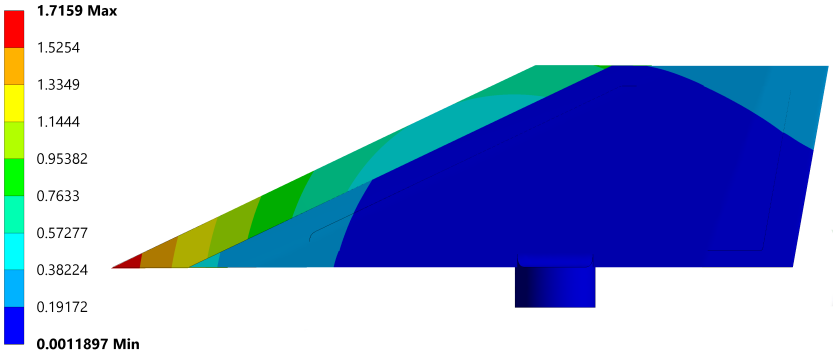


Fig. 17: Contours of maximum displacement (mm)

loads experienced by the wing at Mach 10 could be quite detrimental as the stresses induced are substantial enough to cause structural failure.

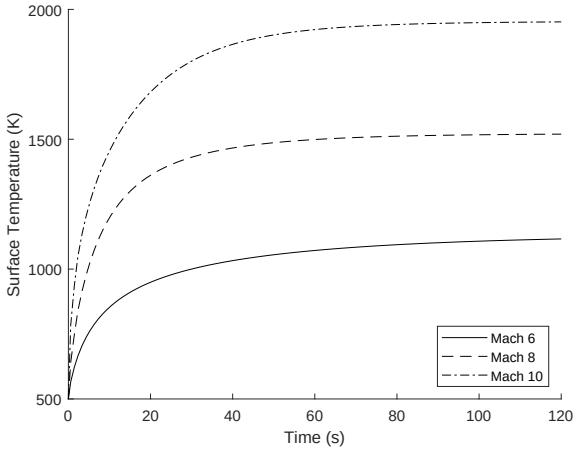


Fig. 18: Surface temperature profile for different cruise velocity

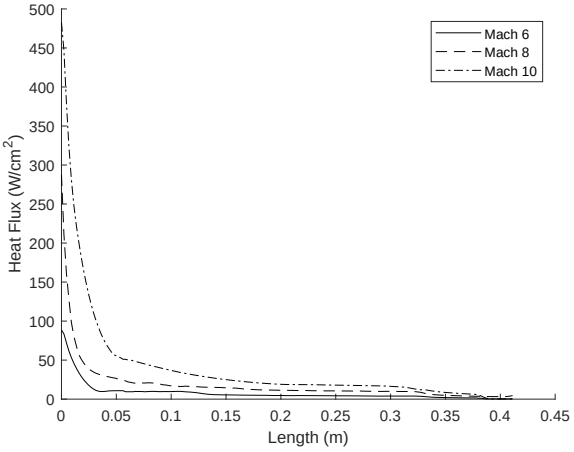


Fig. 19: Distribution of heat flux along chord length for different flight Mach numbers

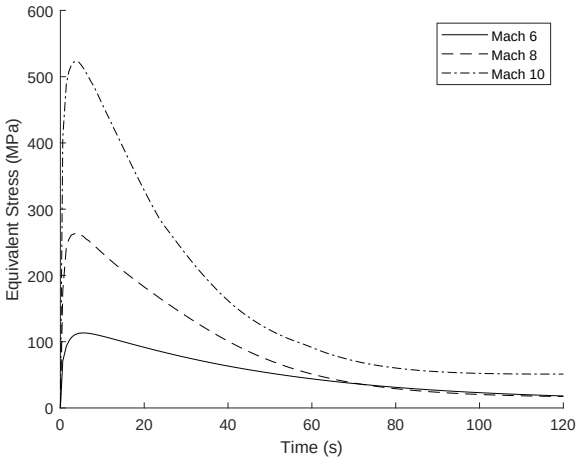


Fig. 20: Equivalent Stress for different cruise velocity

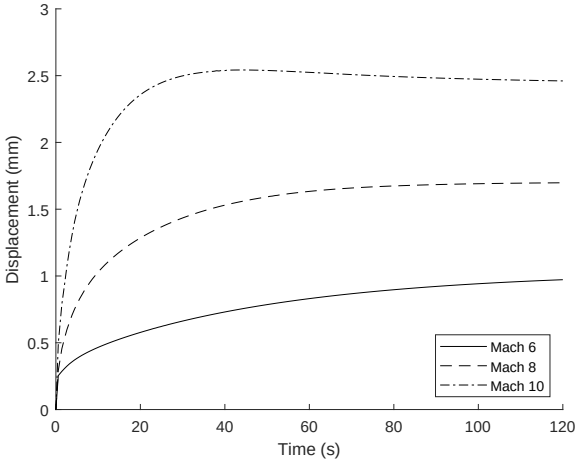


Fig. 21: Maximum displacement for different cruise velocity

4. Conclusion

The aim of the present article was to investigate the performance of the UHTC composite-based hot structure TPS for the control surface. The problem of aerodynamic heating associated with hypersonic flight has been of primary interest for decades. Various methods of thermal protection systems were developed to mitigate this detrimental effect of high-speed compressible flows. In the recent past, the concept of hot structure TPS has become a subject of extensive research due to innovations in ultra-high-temperature ceramic composites. The outcomes in this paper offer a unique perspective on the potential of UHTCC-based TPS for the hypersonic air-breathing vehicle through uncoupled multiphysics simulations.

1. The results of hypersonic flow analysis showed that with increasing flight velocity, the aerothermal effects on the vehicle become far more substantial. Furthermore, a lower cruise altitude could also result in higher aerodynamic heating.

2. The UHTC composites are viable materials for reusable hot structure thermal protection systems for hypersonic cruise vehicles due to their low density, high strength and resistance to high temperatures.

3. The high emissivities of UHTC composites help lower the temperatures by surface radiative cooling. This phenomenon played a key role in mitigating excessive heating of the control surface structure. A significant amount of isothermal heat flux was lost by radiation and the net heat flux to the vehicle was about 287 W/cm^2.

4. An uncoupled approach toward aerothermal and structural analysis was found to be computationally inexpensive and faster than the coupled method and can be used to analyse the behaviour of hot structures effectively.

The results obtained from aerothermal and structural analysis were validated through literature and grid convergence tests. Taken together, our findings and the findings of previous studies point towards the importance of developing a viable and reusable thermal protection system for longer and endurable hypersonic flights. Besides, accurate numerical methods are imperative to account for the effects of hypersonic flow accurately.

The most important limitation of our study is that it is entirely numerical and considers aerothermal effects only. Future research may extend this work by testing UHTC composite-based hot structures for various flight conditions to further study their structural viability for hypersonic air-breathing vehicles.

Acknowledgement

The authors acknowledge help received from the members of DOFS, Defence Research and Development Laboratory.

Nomenclature

Symbol	Description
ρ	Density (kg/m^3)
t	Time (s)
u, v, w	Velocity components in x, y and z-direction (m/s)
p	Pressure (Pa)
τ	Shear stress tensor
e	Internal energy
k	Thermal Conductivity
$\dot{q}_{cond-net}$	Net conducted heat flux (W/m^2)
$\dot{q}_{conv}$	Convected heat flux to structure (W/m^2)
$\dot{q}_{rad-in}$	Radiation heat in-flux (W/m^2)
$\dot{q}_{rad-out}$	Radiation heat out-flux (W/m^2)
h	Heat transfer coefficient (W/m^2K)
σ	Stefan-Boltzmann constant ($5.67\times10^{-8}W/m^2K^4$)
ϵ	Emissivity
c_p	Constant pressure specific heat (J/kg.K)
T_{aw}	Adiabatic wall temperature (K)
T_{iso}	Isothermal wall temperature (K)
TPS	Thermal Protection System
UHTCC	Ultra-High-Temperature Ceramic Composite
NASP	National Aerospace Plane
FGM	Functionally Graded Materials
CMC	Ceramic Matrix Composite
MMC	Metal Matrix Composite
TSR	Thermal Shock Resistance

References

[1] S. Kasen, Thermal Management at Hypersonic Leading Edges, (2013).

[2] C. P. Leonard, R. M. Amundsen, B. Walter, Hyper-X Hot Structures Design and Comparison With Flight Data, AIAA/CIRA 13th International Space Planes and Hypersonic Systems and Technologies, (2005).

[3] C. Wang, F. Li, Z. C. Ding, L. Zhang, Numerical simulation of hypersonic flow around an aerospace plane by Parallel RANS based CFD, Procedia Engineering, Vol. 61, (2013).

[4] S. Narendar, R. Gopikrishna, Evaluation of structural integrity of tactical missile ceramic radomes under combined thermal and structural loads, Procedia Structural Integrity, Vol. 14, (2019).

[5] J. Manu, G. Vinod, R. N. Mathews, Thermo-Structural Analysis of Thermal Protection System for Re-Entry Module of Human Space Flight, Vol. 5, (2016), 125–137.

[6] B. Esser, J. Barcena, M. Kuhn, A. Okan, L. Haynes, S. Gianella, A. Ortona, V. Liedtke, D. Francesconi, H. Tanno, Innovative thermal management concepts and material solutions for future space vehicles, Journal of Spacecraft and Rockets, Vol. 53, (2016), 1051–1060.

[7] Q. Lu, G. Jiang, X. Zhang, D. Deng, Design of lightweight graded hot structures for hypersonic vehicles, (2013), 838–841.

[8] D. E. Glass, Ceramic Matrix Composite (CMC) Thermal Protection Systems (TPS) and Hot Structures for Hypersonic Vehicles, 15th AIAA International Space Planes and Hypersonic Systems and Technologies Conference, (2008), 1–36.

[9] A. Purwar, Thermo-structural Design of Hypersonic Vehicle Sharp Leading Edges for Thermo-erosive Stability Using Finite Element Modelling, 31st International Symposium on Shock Waves 2, (2019), 1027–1034.

[10] D. R. Tenney, Materials and Structures for Hypersonic Vehicles, Journal of Aircraft, (1989).

[11] W. Krenkel, Carbon Fibre Reinforced Silicon Carbide Composites (C/SiC, C/C-SiC), Handbook of Ceramic Composites, (2006), 117–148.

[12] T. Reimer, I. Petkov, D. Koch, M. Fried, C. Dellin, Fabrication and Characterization of C/C-SiC Material made with Pitch-based Carbon Fibers, (2015), 1–17.

[13] W. Li, T. Cheng, D. Li, D. Fang, Numerical Simulation for Thermal Shock Resistance of Ultra-High Temperature Ceramics Considering the Effects of Initial Stress Field, Vol. 2011, (2011).

[14] A. Viviani, G. Pezzella, Aerospace Technology Aerodynamic and Aerothermodynamic Analysis of Space Mission Vehicle, (2015).

[15] E. H. Hirschel, Basics of Aerothermodynamics, (2005).

[16] A. Nisar, R. Hassan, A. Agarwal, K. Balani, Ultra-high temperature ceramics: Aspiration to overcome challenges in thermal protection systems, Ceramics International, Vol. 48, (2022), 8852–8881.

[17] M. Dharavath, P. Manna, D. Chakraborty, Tip-to-tail numerical simulation of a hypersonic air-breathing engine with ethylene fuel, Acta Astronautica, Vol. 128, (2016), 107–118.

[18] T. K. S. Murthy, Computational Methods in Hypersonic Aerodynamics, Kluwer Academic Publishers, (1991).

[19] L. Fu, M. Karp, S. T. Bose, P. Moin, J. Urzay, Shock-induced heating and transition to turbulence in a hypersonic boundary layer, (2020).

[20] R. Stadelmann, ZrB2-SiC based ultra high temperature ceramic composites: Mechanical performance and measurement and design of thermal residual stresses for hypersonic vehicle applications, (2015).

[21] X. Sun, H. Yang, T. Mi, Thermo-Structural Behaviour Prediction of the Nose Cap of a Hypersonic Vehicle Based on Multifield Coupling, International Journal of Aerospace Engineering, Vol. 2020, (2020).

[22] F. Chen, H. Liu, S. Zhang, Coupled heat transfer and thermo-mechanical behavior of hypersonic cylindrical leading edges, International Journal of Heat and Mass Transfer, Vol. 122, (2018), 846–862.

[23] A. Rasouli, H. Toopchi-Nezhad, Coupled vs uncoupled analysis of one-way RC-slabs under nearby air explosions, International Journal of Advanced Structural Engineering, Vol. 10, (2018), 421–437.

[24] T. J. Coakley, C. C. Horstman, J. G. Marvin, J. R. Viegas, J. E. Bardina, M. I. Kussoy, M. Field, P. G. Huang, Turbulence Compressibility Corrections, (1994).

[25] R. G. J. Sager, Compressible dissipation, pressure dilation and pressure induced diffusion in hypersonic turbulence modeling, Vol. 9, (1996).

[26] C. Hu, Y. Sakka, B. Jang, H. Tanaka, T. Nishimura, S. Guo, S. Grasso, Microstructure and properties of ZrB2-SiC and HfB2-SiC composites fabricated by spark plasma sintering (SPS) using TaSi2 as sintering aid, Journal of the Ceramic Society of Japan, Vol. 118, (2010), 997–1001.

[27] S. Meng, H. Chen, J. Hu, Z. Wang, Radiative properties characterization of ZrB2-SiC-based ultrahigh temperature ceramic at high temperature, Materials and Design, Vol. 32, (2011), 377–381.

[28] M. May, G. D. Rupakula, P. Matura, Non-polymer-matrix composite materials for space applications, Composites Part C: Open Access, Vol. 3, (2020).

[29] R. Luo, T. Liu, J. Li, H. Zhang, Z. Chen, G. Tian, Thermophysical properties of carbon/carbon composites and physical mechanism of thermal expansion and thermal conductivity, Carbon, Vol. 42, (2004), 2887–2895.

[30] M. Patel, K. Saurabh, V. V. B. Prasad, J. Subrahmanyam, High temperature C/C-SiC composite by liquid silicon infiltration: a literature review, Bull. Mater. Sci, Vol. 35, (2012), 63–73.